

LONDON
SCHOOL of
HYGIENE
& TROPICAL
MEDICINE



Pearson, JS; Giogha, C; Mhlen, S; Nachbur, U; Pham, CL; Zhang, Y; Hildebrand, JM; Oates, CV; Lung, TW; Ingle, D; Dagley, LF; Bankovacki, A; Petrie, EJ; Schroeder, GN; Crepin, VF; Frankel, G; Masters, SL; Vince, J; Murphy, JM; Sunde, M; Webb, AI; Silke, J; Hartland, EL (2017) EspL is a bacterial cysteine protease effector that cleaves RHIM proteins to block necroptosis and inflammation. *Nature microbiology*, 2. p. 16258. ISSN 2058-5276 DOI: <https://doi.org/10.1038/nmicrobiol.2016.258>

Downloaded from: <http://researchonline.lshtm.ac.uk/4646423/>

DOI: [10.1038/nmicrobiol.2016.258](https://doi.org/10.1038/nmicrobiol.2016.258)

Usage Guidelines

Please refer to usage guidelines at <http://researchonline.lshtm.ac.uk/policies.html> or alternatively contact researchonline@lshtm.ac.uk.

Available under license: <http://creativecommons.org/licenses/by-nc-nd/2.5/>

1 **EspL is a bacterial cysteine protease effector that cleaves RHIM proteins to block necroptosis**
2 **and inflammation**

3

4 Jaelyn S. Pearson^{1*}, Cristina Giogha^{1*}, Sabrina Mühlen^{1[∞]}, Ueli Nachbur^{2,3}, Chi L. L. Pham⁴, Ying
5 Zhang¹, Joanne M. Hildebrand^{2,3}, Clare V. Oates¹, Tania Wong Fok Lung¹, Danielle Ingle¹, Laura
6 F. Dagley^{2,3}, Aleksandra Bankovacki^{2,3}, Emma J. Petrie^{2,3}, Gunnar N. Schroeder^{5^}, Valerie F.
7 Crepin⁵, Gad Frankel⁵, Seth L. Masters^{2,3}, James Vince^{2,3}, James M. Murphy^{2,3}, Margaret Sunde⁴,
8 Andrew I. Webb^{2,3}, John Silke^{2,3} and Elizabeth L. Hartland^{1#}

9 *equal contribution

10

11 ¹Department of Microbiology and Immunology, University of Melbourne at the Peter Doherty
12 Institute for Infection and Immunity, Melbourne 3000, Australia

13 ²The Walter and Eliza Hall Institute of Medical Research, Parkville, Victoria 3052, Melbourne,
14 Australia

15 ³Department of Medical Biology, University of Melbourne, Victoria 3010, Australia

16 ⁴Discipline of Pharmacology, School of Medical Sciences, University of Sydney, New South Wales
17 2006, Australia

18 ⁵MRC Centre for Molecular Bacteriology and Infection, Department of Life Sciences, Imperial
19 College London, SW7 2AZ, UK

20

21 [∞] Current address: Department of Molecular Infection Biology, Helmholtz-Centre for Infection
22 Research, 38124 Braunschweig, Germany

23 [^] Current address: Centre for Experimental Medicine, Queen's University Belfast, BT9 7BL, UK

24

25 [#]Correspondence: hartland@unimelb.edu.au

26

27 **Manuscript information:**

28 **Word count:** 1420

29 **Running title:** Type III effector EspL blocks necroptosis

30 **Keywords:** EPEC/necroptosis/RHIM/cysteine protease

31

32 Cell death signalling pathways contribute to tissue homeostasis and provide innate protection
33 from infection. Adaptor proteins such as RIPK1, RIPK3, TRIF and ZBP1/DAI that contain
34 receptor-interacting protein (RIP) homotypic interaction motifs (RHIM) play a key role in
35 cell death and inflammatory signalling¹⁻³. RHIM-dependent interactions help drive a caspase-
36 independent form of cell death termed necroptosis^{4,5}. Here we report that the bacterial
37 pathogen enteropathogenic *Escherichia coli* (EPEC) uses the type III secretion system (T3SS)
38 effector EspL to degrade the RHIM containing proteins, RIPK1, RIPK3, TRIF and
39 ZBP1/DAI during infection. This required a previously unrecognised tripartite cysteine
40 protease motif in EspL (Cys⁴⁷, His¹³¹, Asp¹⁵³) that cleaved within the RHIM of these proteins.
41 Bacterial infection and/or ectopic expression of EspL led to rapid inactivation of RIPK1,
42 RIPK3, TRIF and ZBP1/DAI and inhibition of TNF, LPS or poly(I:C)-induced necroptosis
43 and inflammatory signalling. Furthermore, EPEC infection inhibited TNF-induced
44 phosphorylation and plasma membrane localization of MLKL. *In vivo*, EspL cysteine
45 protease activity contributed to persistent colonization of mice by the EPEC-like mouse
46 pathogen *Citrobacter rodentium*. The activity of EspL defines a family of T3SS cysteine
47 protease effectors found in a range of bacteria and reveals a mechanism by which
48 gastrointestinal pathogens directly target RHIM-dependent inflammatory and necroptotic
49 signalling pathways.

50

51 RHIM containing proteins, including RIPK1, RIPK3, TRIF and ZBP1/DAI, play essential roles in
52 the regulation of inflammatory and cell death-signalling pathways⁵. RIPK1 is a key regulator of the
53 NF- κ B signalling pathway in response to TNF/TNFR1 stimulation, and may induce apoptosis
54 through formation of a cytosolic complex containing TRADD/FADD and caspase-8⁶. However,
55 upon inhibition of caspase-8 activity, RIPK1 binds RIPK3 through RHIM-RHIM interactions
56 leading to phosphorylation of RIPK3 and the recruitment and phosphorylation of MLKL by

57 activated RIPK3⁷⁻¹¹. Phosphorylated oligomeric MLKL translocates to the plasma membrane,
58 which leads to the caspase independent form of cell death termed necroptosis^{12,13}. Necroptosis may
59 also result from TRIF or DAI/ZBP1 interactions with RIPK1 and RIPK3, which are also mediated
60 by RHIM-RHIM interactions^{14,15}. In addition, RIPK3 can promote NLRP3 inflammasome
61 activation independently of necroptosis that is thought to be triggered by RHIM-RHIM amyloid
62 formation¹⁶.

63

64 Infection of intestinal epithelial cells with the attaching and effacing enteropathogen, EPEC, leads
65 to rapid inhibition of host inflammatory and apoptosis signalling pathways due to the activity of
66 T3SS effectors¹⁷. While studying the effect of EPEC infection on assembly of the TNFR1 receptor
67 complex, we observed that RIPK1 was rapidly degraded during wild type EPEC infection
68 (E2348/69) but not during infection with the T3SS mutant (*ΔescN*) (Supplementary Figure 1a). By
69 testing derivatives of EPEC lacking the genomic islands *PP4* alone (*ΔPP4*) or *PP4* and *IE6*
70 (*ΔPP4/IE6*), we identified *IE6* and subsequently the gene encoding the effector EspL as essential
71 for T3SS-dependent RIPK1 degradation (Fig. 1a; Supplementary Figure 1b). *espL* is located
72 upstream of the T3SS effector genes, *nleB1* and *nleE*, which encode known inhibitors of apoptosis
73 and NF-κB activation respectively (Fig. 1a)¹⁸⁻²⁰. We confirmed that EspL was translocated by the
74 T3SS using the TEM1 β-lactamase reporter²¹ and that deletion of *espL* had no impact on actin
75 accretion by EPEC, a measure of adherence and T3SS activity (Supplementary Figure 1c-e).

76

77 In mammalian cells, RIPK1 may be removed by K48-linked ubiquitylation and proteosomal
78 degradation or by caspase-mediated cleavage²²⁻²⁴. However, neither caspase nor proteasome
79 inhibitors, z-VAD-FMK (z-VAD) and MG132 respectively, prevented EspL-dependent loss of
80 RIPK1 (Fig. 1b). Therefore, we speculated that EspL might mediate direct degradation of RIPK1.

81 Although amino acid sequence analysis failed to uncover any canonical protease motifs, alignment

82 of EspL with homologues identified by BLAST²⁵ from a range of bacterial pathogens revealed a
83 putative conserved cysteine protease motif with the possible catalytic residues Cys⁴⁷, His¹³¹ and
84 Asp¹⁵³ (Fig. 1c, d, 2a; Supplementary Figure 2). Despite lacking primary amino acid sequence
85 similarity with known cysteine proteases, the secondary structure of EspL predicted by Phyre²⁶
86 showed N-terminal similarity to the CA clan of papain-like cysteine proteases, which includes the
87 unrelated T3SS effector YopT from *Yersinia* spp. (Fig. 1c)²⁷. Despite this, the broad spectrum
88 cysteine protease inhibitors, antipain and Z-FA-FMK had no or only weak effect on EspL activity
89 (Supplementary Figure 1f). Complementation of EPEC strain Δ PP4/IE6 or the Δ espL mutant with
90 native EspL expressed *in trans* restored RIPK1 degradation. However, alanine substitution of Cys⁴⁷,
91 His¹³¹ and Asp¹⁵³ but not Cys⁴⁰ abrogated EspL-induced RIPK1 degradation, confirming the crucial
92 role of these amino acids in EspL activity (Fig. 1d).

93

94 To determine the specificity of EspL for RIPK1 degradation, we examined the effect of EPEC
95 infection on human as well as murine RIP kinases by immunoblot. In addition to RIPK1,
96 catalytically active EspL also induced loss of RIPK3, which shares a high degree of similarity with
97 RIPK1²⁸ (Fig. 1d, Supplementary Figure 3a). Levels of RIPK2 were unaffected by EspL. Using an
98 antibody generated to residues 385-650 of RIPK1, we detected a ~14 kDa cleavage product
99 following ectopic expression of codon optimised Flag-EspL in HEK293T cells, suggesting that
100 EspL removed the C-terminus of RIPK1 which encompasses the RHIM (Supplementary Figure 3b).
101 To test the ability of EspL to cleave all mammalian RHIM containing proteins directly, we
102 incubated purified recombinant EspL with the purified RHIM-containing regions of RIPK1, RIPK3,
103 TRIF and ZBP1 and observed cleavage by catalytically active EspL for all RHIM proteins (Fig. 2b).
104 Intact mass spectrometry and N-terminal sequencing of the cleavage products from RIPK3 and
105 TRIF identified the cleavage site as QxGxx↓N (P5-P4-P3-P2-P1-P1') (Fig. 2b, c, Supplementary
106 Figure 3c, d). Substitution of V⁴⁴⁸, Q⁴⁴⁹, I⁴⁵⁰ and G⁴⁵¹ with alanine abrogated the ability of EspL to

107 cleave RIPK3 during EPEC infection suggesting that this conserved RHIM sequence was important
108 for substrate recognition by EspL (Supplementary Figure 3e). EspL also possessed the ability to
109 cleave the viral RHIM containing protein M45 from MCMV (Supplementary Figure 3f).

110

111 Given the observed cleavage of RIPK1 and RIPK3, we hypothesised that EspL would prevent
112 RIPK1/RIPK3-dependent necroptosis. Mouse dermal fibroblasts (MDF) were used to create stable,
113 doxycycline inducible cell lines expressing EspL or EspL_{C47S}. Induction of catalytically active EspL
114 was coincident with loss of RIPK1 and RIPK3 and this effect was reversible upon removal of
115 induction (Supplementary Figure 4a, b). Cells expressing EspL were protected from necroptotic cell
116 death, as measured by PI uptake, when induced by treatment with TNF, QVD or z-VAD (as caspase
117 inhibitors) and the Smac-mimetic IAP antagonist, compound A (Cp.A) as an inhibitor of NF- κ B
118 activation²⁹. These conditions are known to induce cell death by necroptosis¹³. This protection
119 required EspL activity (Supplementary Figure 4c, 5a, b). EspL expression in MDF cells also
120 prevented MLKL oligomerization and membrane translocation (Supplementary Figure 5c), two
121 hallmarks of necroptosis¹³. During infection, EPEC blocked MLKL phosphorylation,
122 oligomerization and membrane translocation and consequently necroptosis in HT-29 cells in an
123 EspL dependent manner (Fig. 3, Supplementary Figure 6).

124

125 Apart from EspL, the T3SS effector NleB1 from EPEC can block TNF induced necroptosis by
126 modifying a conserved arginine in the death domain of RIPK1 with *N*-acetyl glucosamine
127 (GlcNAc)¹⁹. Consistent with partial redundancy in EspL and NleB1 function, only EPEC
128 derivatives lacking both *espL* and *nleB1* ($\Delta PP4/IE6$ or $\Delta espLnleBE$) were unable to inhibit TNF-
129 induced necroptosis (Fig. 3b; Supplementary Figure 6). In addition, complementation of $\Delta PP4/IE6$
130 with either active EspL or NleB but not NleE, restored EPEC-mediated inhibition of necroptosis

131 whereas inactive EspL (EspL_{C47S}) or NleB1 (NleB1_{AAA})^{18,19} did not (Fig. 3, Supplementary Figure
132 6).

133

134 Consistent with loss of RIPK1, ectopic expression of EspL, but not inactive EspL, blocked TNF-
135 induced expression of an NF-κB dependent luciferase reporter (Supplementary Figure 7a). In
136 addition, EspL delivered by the T3SS in the EPEC mutant background *ΔPP4/IE6* resulted in
137 reduced IL-8 production by infected HT-29 cells (Supplementary Figure 7b). EspL dependent loss
138 of TRIF following EPEC infection or ectopic expression resulted in impaired interferon-β (*Inffβ*)
139 expression and necroptosis induced by the TLR3 and TLR4 ligands, poly(I:C) and LPS,
140 respectively (Fig. 4a, b, Supplementary Figure 7c). Using immortalised bone marrow derived
141 macrophages (iBMDM), we observed that EspL blocked NLRP3/RIPK3-dependent caspase-1
142 activation induced by treatment with Cp.A/QVD¹⁶, whereas activation of the canonical NLRP3
143 inflammasome by nigericin was unaffected (Supplementary Figure 7d).

144

145 Although EspL possessed the ability to cleave all mammalian RHIM-containing proteins, a time
146 course comparing RIPK1 and RIPK3 cleavage suggested that RIPK1 was the preferred target
147 during EPEC infection (Supplementary Figure 8a). In addition, cleavage likely occurred before
148 amyloid formation as RHIM fibrils were only inefficiently cleaved by EspL compared to the
149 monomeric proteins (Supplementary Figure 8b, c). Amyloid fibrils form the signalling scaffold of
150 the necrosome and arise from RHIM-RHIM interactions between RIPK1 and RIPK3⁴.

151

152 The targeted inhibition of necroptosis and RHIM-dependent inflammatory signalling by EspL
153 during EPEC infection suggested that the activity of EspL might aid mucosal immune evasion. Here
154 we assessed the ability of derivatives of the EPEC-like mouse pathogen, *C. rodentium* to colonise
155 wild type C57BL/6 mice. *C. rodentium* is a murine attaching and effacing pathogen that carries all

156 the conserved T3SS effector genes present in EPEC, including *espL*. We confirmed that EspL from
157 *C. rodentium* (CREspL) cleaved RIPK1, whereas inactive CREspL_{C42S} did not (Fig. 4c). In wild
158 type C57BL/6 mice, we observed that an *espL* mutant of *C. rodentium* was attenuated for intestinal
159 colonization in the resolving phase of infection suggesting that EspL promoted bacterial persistence
160 in the gut, similar to previous findings³⁰ (Supplementary Figure 9). Complementation of the *espL*
161 mutant with *espL* but not *espL*_{C47S} restored intestinal colonization by *C. rodentium* (Fig. 4d)
162 suggesting that the cysteine protease activity of EspL was critical to its virulence function. Given
163 the semi-redundant activities of EspL and NleB1 that we observed in the inhibition of necroptosis,
164 and the fact that *nleB* mutants of *C. rodentium* also exhibit a colonization defect^{18,19}, further work
165 should examine the relative contribution of each effector in vivo using an *espL/nleB* double mutant
166 of *C. rodentium* complemented with active and inactive forms of NleB and EspL.

167

168 Here we have defined EspL from EPEC as the prototypic member of a family of T3SS cysteine
169 protease effectors and identified the targets of EspL as host RHIM-containing proteins. EspL
170 inactivated inflammatory, inflammasome and necroptotic signalling by cleaving within the RHIM,
171 thereby disrupting a range of host mucosal defence pathways. EspL adds to the arsenal of bacterial
172 T3SS effectors that subvert host cell signalling and the presence of, as yet uncharacterised, EspL
173 homologues in a broad range of bacterial pathogens suggests that this family of cysteine protease
174 effectors constitutes a widespread virulence mechanism.

175

176 **Acknowledgments**

177 We gratefully acknowledge Edward Mocarski (Emory University) for the gift of Flag-ZBP1/DAI
178 and Flag-M45 and Gabrielle Belz (Walter and Eliza Hall Institute) for animal ethics assistance. We
179 thank Sam Young (Walter and Eliza Hall Institute) for technical assistance. This work was
180 supported by the Australian National Health and Medical Research Council (Program Grant

181 ID606788 to ELH, Project Grants APP1057888 to JS and APP1051210 to JV and APP1057905 to
182 JMM and JS; Fellowships APP1090108 to JSP, APP1052598 to JV and APP1105754 to JMM) and
183 the Australian Research Council (Future Fellowship FT130100166 to UN, Discovery Project
184 DP150104227 to MS). CG and DI were supported by Australian Postgraduate Awards. TW was
185 supported by a University of Melbourne International Research Scholarship (MIRS). GNS is funded
186 by the Medical Research Council, UK. This work was made possible through Victorian State
187 Government Operational Infrastructure Support and Australian Government NHMRC IRIISS. The
188 authors declare no financial interests related to this work.

189

190 **Author contributions.** J.S.P., C.G., S. M., U. N, C.L.L.P., Y.Z., J.M.H., T.W., D. I., A.B., E. J. P.
191 J.V. and M.S. designed and performed the experiments. S.L.M., J.M., G.N.S., C.V.O., V.F.C. and
192 G.F contributed reagents and expertise. L.F.D. and A.I.W. performed mass spectrometry analyses.
193 J.S.P. C. G, J.S. and E.L.H. designed the experiments and wrote the manuscript.

194

195 **METHODS**

196 **Bacterial strains, plasmids, cell lines and growth conditions**

197 The bacterial strains, plasmids and oligonucleotide primers used in this study are listed in
198 Table S1. Bacteria were grown at 37 °C in Luria-Bertani (LB) medium, Dulbecco's Modified
199 Eagle's medium (DMEM) with GlutaMAX (Gibco, NY), or Roswell Park Memorial Institute
200 medium (RPMI) with GlutaMAX (Gibco) where indicated and supplemented with ampicillin (100
201 µg/mL), kanamycin (100 µg/mL), nalidixic acid (50 µg/mL) or chloramphenicol (25 µg/mL) where
202 necessary.

203 Mouse dermal fibroblasts (MDFs) were isolated from the dermis of adult mice and
204 immortalised with SV40 large T antigen³¹. Bone marrow derived macrophages from C57BL/6
205 mice were immortalized to generate a macrophage cell line (iBMDM) with CreJ2 virus as described
206 previously³². All other cell lines were sourced from and authenticated by either the ATCC Global
207 Bioresource Centre, or the ECACC via Sigma-Aldrich. HeLa cells, HEK293T cells, Caco-2 cells,
208 iBMDMs, MDFs and MEFs were grown in DMEM GlutaMax (Gibco) supplemented with 10%
209 FCS (Sigma) at 37 °C with 5% CO₂. HT-29 cells were grown in Roswell Park Memorial Institute
210 medium (RPMI) GlutaMAX (Gibco) with 10% FCS (Sigma) at 37 °C with 5% CO₂.

211 **Construction of EspL expression vectors**

212 For expression in bacteria, the *espL* gene was amplified from EPEC E2348/69 genomic
213 DNA by PCR using the primer pair EspL_F/EspL_R for cloning into pTrc99A. PCR amplification
214 consisted of an initial denaturation step at 95 °C for 10 min, followed by 30 cycles of 94 °C for 44
215 sec, 55 °C for 45 sec and 70 °C for 2 min followed by a final elongation step of 70°C for 10 min.
216 The PCR product was digested with KpnI and EcoRI and ligated into pTrc99A to produce pEspL.

217 For expression in mammalian cells, the gene encoding EspL from either EPEC E2348/69 or
218 *C. rodentium* ICC169 was codon-optimised (DNA2.0), amplified using the primer pair
219 EspL_{COF}/EspL_{COR} or EspL_{CRCOF}/EspL_{CRCOR} and ligated into KpnI/BamHI digested p3XFlag-MyC-

220 CMV-24 to generate N-terminal 3xFlag fusions of EspL (pFlag-EspL or pFlag-CREspL). For
221 construction of the lentiviral plasmid to generate stable inducible cell lines, codon optimised Flag-
222 EspL was amplified from pFlag-EspL and ligated into pF TRE3G PGK puro^{10,29} using
223 BamHI/XbaI.

224 Genes encoding residues 2-549 of EPEC E2348/68 EspL and EspL_{C47S} were amplified by
225 PCR using pEspL and pEspL_{C47S} as template DNA respectively, using the primer pair
226 EspL_{GEXF}/EspL_{GEXR}. PCR products were digested with BamHI and NotI and ligated into the vector
227 pGEX-2T-TEV, as previously described³³ to enable bacterial expression with an in-frame N-
228 terminal GST fusion. Insert sequences were verified by Sanger sequencing (Micromon, Monash
229 University, Australia).

230 **Site-directed mutagenesis**

231 Site-directed mutants were generated using the Stratagene QuikChange II Site-Directed
232 Mutagenesis Kit according to manufacturer's protocol. pEspL_{C40S}, pEspL_{C47S}, pEspL_{H131A},
233 pEspL_{D153A} were generated using pEspL as template DNA and primer pairs EspL_{(C40S)F}/EspL_{(C40S)R},
234 EspL_{(C47S)F}/EspL_{(C47S)R}, EspL_{(H131A)F}/EspL_{(H131A)R} and EspL_{(D153A)F}/EspL_{(D153A)R} respectively. pFlag-
235 EspL_{C40S}, pFlag-EspL_{C47S}, pFlag-EspL_{H131A}, pFlag-EspL_{D153A} were generated using pFlag-EspL as
236 template DNA and primer pairs EspL_{(C40S)COF}/EspL_{(C40S)COR}, EspL_{(C47S)COF}/EspL_{(C47S)COR},
237 EspL_{(H131A)COF}/EspL_{(H131A)COR} and EspL_{(D153A)COF}/EspL_{(D153A)COR} respectively. pF TREG-Flag-
238 EspL_{C47S} was generated using pF TREG-Flag-EspL as template DNA and primer pair
239 EspL_{(C47S)COF}/EspL_{(C47S)COR}. pFlag-CREspL_{C42S} was generated using pFlag-CREspL as template
240 DNA and primer pair EspL_{C42S(CO)F}/EspL_{C42S(CO)R}. pGEX-EspL_{C47S} was generated by PCR-
241 amplification of a cDNA encoding EPEC E2348/69 EspL_{C47S} (pTrc-EspL_{C47S}) using primers
242 EspL_{GEXF}/EspL_{GEXR} bearing restriction sites (5' BamHI, 3' NotI), followed by restriction digest and
243 ligation into the vector, pGEX-2T-TEV (pGEX-EspL_{C47S}). pGFP-mRIPK3_{AAAA} was generated
244 using pGFP-mRIPK3 as template DNA and primer pair mRIPK3_{AAAA-F}/mRIPK3_{AAAA-R}.

245 **Purification of GST-EspL**

246 600 mL Super broth cultures containing 100 µg/mL ampicillin were inoculated with *E. coli*
247 BL21 Codon Plus transformed with GST-EspL or GST-EspL_{C47S} expression constructs and cultured
248 at 37 °C with shaking to OD₆₀₀ of 0.6-0.8. Cultures were then cooled to 18 °C, protein expression
249 induced by addition of 1 mM IPTG with continued shaking and incubation at 18 °C overnight. Cell
250 pellets were resuspended in lysis buffer (200 mM NaCl, 20 mM HEPES pH 7.5, 5% w/v glycerol,
251 0.5 mM TCEP), before lysis by sonication, elimination of debris by centrifugation at 45000 g, 0.45
252 µm filtration of the lysate and incubation with glutathione agarose (UBP Bio) at 4 °C with agitation
253 for 1-2 h. Beads were collected and washed with lysis buffer before incubation with 200 µg TEV
254 protease at 20 °C for 2 h on rollers. Supernatant containing cleaved EspL or EspL_{C47S} was
255 concentrated by centrifugal ultrafiltration and loaded on to Superdex S200 gel filtration column pre-
256 equilibrated with gel filtration buffer (200 mM NaCl, 20 mM HEPES pH 7.5, 5% v/v glycerol).
257 Fractions containing purified EspL or EspL_{C47S}, as assessed by SDS-PAGE, were pooled,
258 concentrated by centrifugal ultrafiltration to 5 mg/mL, aliquoted, snap frozen in liquid nitrogen and
259 stored at -80 °C until required.

260 **RHIM domain protein constructs, expression and purification**

261 Synthetic genes encoding RHIM-containing regions of human RIPK1 (Q13546; residues
262 497-583), human RIPK3 (Q9Y572; residues 387-518), human DAI/ZBP1 (Q9H171; residues 170-
263 429), human TRIF (Q8IUC6; residues 601-712) with flanking BamHI and EcoRI restriction sites
264 were purchased from Genscript, digested with these restriction enzymes, purified by agarose gel
265 electrophoresis and ligated individually into the pHUE vector cut with the same two restriction
266 enzymes³⁴. All expressed fusion proteins therefore consist of His6-ubiquitin-RHIM region.
267 Successful cloning was confirmed by sequencing at AGRF (Westmead Institute) Sydney. Proteins
268 were expressed in BL21(DE3) grown at 37 °C to an OD₆₀₀ of 0.6-0.8, and induced with 0.5 mM
269 IPTG for 3 h. Cell pellets were lysed in 6M GuHCl, 100 mM NaH₂PO₄, 20 mM Tris.Cl, 5 mM β

270 mercaptoethanol, pH 8.0, and soluble material further purified on Ni-NTA agarose under denaturing
271 conditions, with exchange into 8 M urea, 100 mM NaH₂PO₄, 20 mM Tris, 5 mM β mercaptoethanol
272 at pH 6.0 for washing and pH 4.0 for elution from the Ni-NTA agarose.

273 **Generation of stable inducible cell lines in mouse dermal fibroblasts (MDF) and immortalized**
274 **bone marrow derived macrophages (iBMDM)**

275 HEK293T cells were seeded at 2 x 10⁵ cells per 10 cm culture dishes and 24 h later were co-
276 transfected with 10 μg of either pF TRE3G-Flag-EspL or pF TRE3G-Flag-EspL_{C47S} along with the
277 helper plasmids pMDL-RRE, pRSV-REV and pVSV-g (5, 2.5 and 3 μg, respectively) using
278 Effectine Transfection Reagent (QIAGEN) for a further 24 h. Culture media was then changed and
279 the cells were incubated for a further 48 h for virus production. Polybrene (5 μg/mL) (Sigma) was
280 added to the cell culture dishes and the virus-containing supernatant was collected and passed
281 through a 0.45 μm filter. Virus-containing supernatant was added to either MDF monolayers or
282 iBMDM monolayers and incubated at 37 °C with 5% CO₂ for 24 h. Infected cells were selected for
283 using increasing concentrations of up to 5 μg/mL of puromycin (Sigma) for at least one week.
284 Expression of Flag-EspL or Flag-EspL_{C47S} in either MDFs or iBMDMs was tested by adding 20
285 ng/mL doxycycline at varying time points followed by immunoblot using anti-Flag antibodies.

286 **Construction of *Citrobacter rodentium* *espL* mutant**

287 A 325 bp upstream region of *espL* was amplified using primer pair Up-EspL-Fw/BamHI-
288 Up-EspL-Rv, and a 500 bp downstream region of *espL* was amplified using primer pair BamHI-
289 Down-EspL-Fw/Down-EspL-Rv. Both fragments were then digested with BamHI, ligated together,
290 and cloned into pGEMT. The non-polar *aphT* cassette³⁵ was then inserted into the BamHI site
291 between the two fragments and the orientation of the *aphT* cassette ascertained by PCR. This
292 construct was then amplified using the primer pair Up-EspL-Fw/Down-EspL-Rv. The PCR
293 products were electroporated into ICC169 containing pKD46 encoding lambda red recombinase³⁶.

294 Transformants were selected on kanamycin agar plates and *espL* deletion confirmed by PCR
295 (Check-EspL-UP-Fw /Down-EspL-Rv) and DNA sequencing.

296 ***cis* complementation of the *Citrobacter rodentium espL* mutant**

297 The *Citrobacter rodentium espL* mutant was *cis* complemented with either WT *espL* or
298 *espL_{C42S}* using the transgene insertion method previously described³⁷. Briefly, the *espL* gene with
299 its native promoter was amplified from *C. rodentium* ICC169 genomic DNA template by PCR
300 using primers EspL_{CRF1}/EspL_{CRR1}, and then ligated into the XmaI/XhoI restriction sites of the
301 pGRG36 vector. The pGRG36-EspL_{C42S} construct was generated by site-directed mutagenesis. The
302 pGRG36-EspL construct was used as template DNA and amplified by PCR using primers
303 EspL_{C42SF}/EspL_{C42SR}. The resulting plasmid was digested with DpnI at 37 °C overnight before
304 transformation into the appropriate *E. coli* strain.

305 The pGRG36-EspL and pGRG36-EspL_{C42S} constructs were confirmed by PCR using
306 primers Tn7_F/Tn7_R, then electroporated into electrocompetent *C. rodentium espL* mutant cells and
307 selected for using 100 ug/mL ampicillin and incubated at 30 °C overnight. Transformants were
308 streaked out once, then grown overnight in LB without antibiotics at 30 °C. Dilutions were prepared
309 and plated on LB and grown overnight at 42 °C. Transposition of the Tn7:*espL/espL_{C42S}* into the
310 *attTn7* insertion site in the *C. rodentium espL* mutant chromosome was confirmed by the absence of
311 the ampicillin resistance marker and PCR using primers CRseq_F/CRseq_R.

312 **Construction of EPEC single and triple deletion mutants**

313 To construct the EPEC E2348/69 *espL* deletion mutant strain, 342-bp and 331-bp fragments
314 were amplified from 5' and 3' flanking sites of *espL* using oligonucleotides EspL_{5'F}/ EspL_{5'R} and
315 EspL_{3'F}/ EspL_{3'R}. The plasmid pKD4 was used as template DNA to amplify the kanamycin cassette
316 using oligonucleotides pKD3-4_F and pKD3-4_R. Overlapping PCR was used to assemble the *espL*
317 flanking regions with the kanamycin cassette construct using oligonucleotides EspL_{5'F} and EspL_{3'R}.
318 Lambda red mediated recombination³⁶ was used to replace the wild type allele with the kanamycin

319 resistance cassette. The cassette was electroporated into wild-type EPEC E2348/69 and positive
320 clones were selected for on LB agar with 25 µg/mL kanamycin. To construct the EPEC E2348/69
321 *espLnleBE* deletion mutant, a 368-bp fragment was amplified from 5' flanking site of *nleB* using
322 oligonucleotides NleB_{5'F}/ NleB_{5'R} and 550-bp fragment was amplified from 3' flanking site of *nleE*
323 using oligonucleotides NleE_{3'F}/ NleE_{3'R}. The plasmid pKD3 was used as template DNA to amplify
324 the chloramphenicol cassette using oligonucleotides pKD3-4_F and pKD3-4_R. Overlapping PCR was
325 used to assemble the *nleB* and *nleE* flanking regions with the chloramphenicol cassette construct
326 using oligonucleotides NleB_{5'F} and NleE_{3'R}. Lambda red mediated recombination³⁶ was used to
327 replace the wild type allele with the chloramphenicol resistance cassette. The cassette was
328 electroporated into EPEC E2348/69 *espL* mutant cells and positive clones were selected for on LB
329 agar with 5 µg/mL chloramphenicol. Deletions were confirmed by PCR with a combination of
330 primers from outside and inside the altered region. Attachment and pedestal formation by parental
331 and mutant strains were confirmed using fluorescence actin staining.

332 **EPEC infection**

333 Cell lines of HeLa, Caco-2, MDF and HT-29 cells are maintained in our laboratory and
334 regularly tested for mycoplasma contamination. Two days prior to infection HeLa, Caco-2, MDF or
335 HT-29 cell monolayers were seeded into 24 well tissue culture trays. One day prior to infection
336 derivatives of EPEC were inoculated into LB broth and grown with shaking at 37 °C overnight. On
337 the day of infection, overnight cultures of EPEC were sub-cultured 1:75 in DMEM GlutaMAX
338 (Gibco) or RPMI GlutaMAX (Gibco) and grown statically for 3 h at 37 °C with 5% CO₂. Where
339 necessary, cells were induced with 1 mM isopropyl-B-D-thiogalactopyranoside IPTG (Sigma) 30
340 min prior to infection. Cells were washed twice with PBS and infected with EPEC grown to an
341 OD_{600nm} of 0.03 for 1-3 h (depending on the experiment). When required, the inhibitors MG132
342 (Sigma) (10 µM), antipain (Sigma) (10, 20 or 40 µg/mL), z-VAD-FMK (Abcam) (25 µM), or z-FA-

343 FMK (Abcam) (10, 20 or 40 μ M) were added to the cells 1 hr prior to infection and kept on for the
344 duration of the infection.

345 **Transfection**

346 All transfections were performed in HEK293T cells using Fugene® 6 (Promega)
347 transfection reagent. Cells were seeded into 24 well tissue culture trays and transfected 24 h later
348 with 1 μ g DNA for a period of ~18 h.

349 **Fluorescent actin stain**

350 HeLa cells were seeded on coverslips and infected as previously described. After infection,
351 cells were washed with PBS, fixed in 4 %PFA in PBS for 30 min and permeabilised in 1% Triton
352 X-100 for another 30 min. Cells were then washed twice with PBS and stained with 4',6-diamidino-
353 2-phenylindole (DAPI, Invitrogen) at 0.5 mg/mL and Phalloidin-Tetramethylrhodamine B
354 isothiocyanate (Sigma) in 3% BSA/PBS for 30 min. Coverslips were mounted onto microscope
355 slides with Prolong Gold anti-fade reagent (Invitrogen). Images were acquired using a Zeiss
356 confocal laser scanning microscope with a 1003/EC Epiplan-Apochromat oil immersion objective.

357 **Immunoblot analysis**

358 For immunoblot analysis following EPEC infection, transfection or induction of stable cell
359 lines, cells were collected and lysed in cold lysis buffer (1% Triton X-100, 50 mM Tris-HCl, pH
360 7.4, 1 mM EDTA, 150 mM NaCl) with Complete Protease Inhibitor (Roche), 2 mM Na₃VO₄, 10
361 mM NaF, 1 mM PMSF and incubated on ice for 10 min to complete lysis. Samples were then
362 pelleted at 4 °C by centrifugation and the supernatants added to 4×Bolt® LDS Sample Buffer
363 (Thermo Fisher), heated to 70 °C for 10 min and resolved on Bolt® 4-12% Bis-Tris Plus Gels
364 (Thermo Fisher) by PAGE. Proteins were transferred to nitrocellulose membranes using an iBlot2
365 Gel Transfer Device (Thermo Fisher) and probed with one of the following primary antibodies:
366 mouse monoclonal anti-RIPK1 (38/RIP) (BD Transduction Laboratories), mouse monoclonal anti-
367 RIPK2/RICK (25/RIG-G) (BD Transduction Laboratories), rabbit polyclonal anti-RIPK3 (Abcam)

368 (for HT-29 cells), rabbit polyclonal anti-RIPK3 (ProSci) (for MDF cells) or rabbit polyclonal anti-
369 TRIF (Cell Signaling), mouse monoclonal anti-Flag M2-HRP (Sigma), mouse monoclonal anti-
370 GFP (7.1 and 13.1) (Roche), mouse monoclonal anti- β -actin (AC-15) (Sigma), mouse monoclonal
371 anti-TRADD (7G8) (Cell Signaling), rabbit polyclonal anti-TRAF2 (Cell Signaling), monoclonal
372 rat anti-mouse MLKL (WEHI-3H1) (WEHI, made in-house), mouse monoclonal anti-TEM1 β -
373 lactamase (8A5.A10) (QED Bioscience) diluted in TBS with 5% BSA (Sigma) and 0.1% Tween
374 (Sigma). Proteins were detected using anti-rabbit or anti-mouse IgG secondary antibodies
375 conjugated to horseradish peroxidase (PerkinElmer) diluted in TBS with 5% BSA (Roche) and
376 0.1% Tween (Sigma) and developed with enhanced chemiluminescence (ECL) western blotting
377 reagent (Amersham). Images were visualised using an MFChemisBis imaging station (DNR, Israel).
378 At least three biological replicates were performed for all experiments.

379 **Cell viability assays (MTT and propidium iodide staining)**

380 For analysis of cell viability using MTT assays, immortalised mouse bone marrow-derived
381 macrophages (iBMDM) stably expressing either EspL or EspL_{C47S} were seeded into 24 well tissue
382 culture plates (Corning) for 18-24 h before being left untreated or treated with 20 ng/mL of LPS (*E.*
383 *coli* 0111:B4) (Sigma) or 50 μ g/mL Poly I:C (for iBMDMs) (Sigma) or 10 μ g/mL high molecular
384 weight Poly I:C (InvivoGen, CA, USA) and 10 μ M z-VAD-FMK (Abcam) for a further 18 h. The
385 cells were washed once with PBS and replaced with DMEM containing 0.1 μ g/mL 3-(4,5-
386 Dimethylthiazol-2-yl)-2,5- diphenyltetrazolium bromide (MTT) (Sigma) for 1 h, after which the
387 medium was removed and 100 μ L of dimethyl-sulfoxide (DMSO; Sigma) was added to each well.
388 After thorough mixing on an orbital shaker for 1 min, the absorbance at 540 nm for each well was
389 obtained using a CLARIOstar microplate reader (BMG Labtech, Germany). Results were obtained
390 from at least 3 independent experiments.

391 For analysis of cell viability by propidium iodide (PI) staining of HT-29 monolayers, cells
392 were seeded into 24 well tissue culture plates with sterile glass coverslips and 48 h later were

393 infected with EPEC derivatives as previously mentioned for 2.5 h followed by 4 h incubation in
394 media supplemented with 50 µg/mL gentamicin and 20 ng/mL TNF (Calbiochem), 500 nM
395 compound A (Cp. A, Tetralogic), 25 µM z-VAD-FMK (Abcam). PI (50 µg/mL) (Sigma) was added
396 for the final 15 min of treatment. Cells were then fixed in 3.7% (wt/vol) formaldehyde (Sigma) in
397 PBS for 10 min and permeabilised with 0.2% Triton (Sigma) for 4 min. 4', 6-diamidino-2-
398 phenylindole (DAPI; Invitrogen) was applied at 0.5 µg/mL in PBS for 10 min. Cells were washed
399 with PBS three times and coverslips were mounted onto microscope slides with Prolong Gold anti-
400 fade reagent (Invitrogen). Images were acquired using a Zeiss confocal laser-scanning microscope
401 with a 100x/EC Epiplan-Apochromat oil immersion objective. Duplicate coverslips were blinded
402 for counting of PI positive cells, and results were obtained from at least 3 independent experiments.

403 For analysis of cell viability by PI staining and confocal microscopy in MDF cells, EspL
404 and EspL_{C47S} expressing lines were induced with 20 ng/mL doxycycline for 2 h followed by 4 h
405 incubation in media supplemented with 20 ng/mL TNF (Calbiochem), 500 nM Cp. A (Tetralogic),
406 25 µM z-VAD-FMK (Abcam). PI, DAPI staining and confocal microscopy were carried out as
407 described above. Duplicate coverslips were blinded for counting of PI positive cells, and results
408 were obtained from at least 3 independent experiments.

409 For analysis of cell viability by PI staining and flow cytometry, MDF-EspL and MDF-
410 EspL_{C47S}, cell lines were induced with 10 ng/mL doxycycline for 1 h followed by 24 h incubation in
411 media supplemented with 100 ng/mL hTNF-Fc produced in house (WEHI), 500 nM Cp. A
412 (Tetralogic), 50 µM QVD-OPH (Abcam). Cell death was assessed with PI staining (1 µg/mL) and
413 quantified using a BD FACSCalibur flow cytometer. Data was analysed using the WEASEL Flow
414 Cytometry Software.

415 **Monitoring MLKL complex formation using BN-PAGE**

416 For MDF cells, 5 x 10⁵ cells (wild type, stably expressing inducible Flag-EspL or Flag-
417 EspL_{C47S}) were used to seed each well of a 6 well tissue culture plate and allowed to attach

418 overnight. Cells were stimulated with 0.5 µg/mL doxycycline for 2 h to induce Flag-EspL
419 expression prior to the addition of 100 ng/mL hTNF-Fc produced in house (WEHI), 500 nM Cp. A
420 (Tetralogic), 25 µM z-VAD-FMK (Abcam) for a further 4 h to induce necroptosis. For HT29 cells,
421 5×10^5 cells were plated in each well of a six well plate and allowed to attach for 48 h. Cells were
422 infected with derivatives of EPEC E2348/69 for 2.5 h followed by stimulation with 20 ng/mL TNF
423 (Calbiochem), 500 nM Cp. A (Tetralogic), 25 µM z-VAD-FMK (Abcam) for a further 5 h to induce
424 necroptosis. Cells were harvested by scraping and permeabilised in MELB buffer (20 mM HEPES
425 (pH 7.5), 100 mM KCl, 2.5 mM MgCl₂, 100 mM sucrose, 0.025% digitonin (BIOSYNTH, Staad,
426 Switzerland) 2 µM N-ethyl maleimide, Complete Protease Inhibitor (Roche) and PhosSTOP
427 phosphatase inhibitor cocktail (Roche)). Cytosolic and crude membrane fractions were separated by
428 centrifugation and the crude membrane fraction further solubilized in MELB buffer containing 1%
429 digitonin and clarified by centrifugation. Digitonin was added to the cytosolic fraction (final 1%
430 w/v) and fractions were resolved on a 4-16% Bis-Tris Native PAGE gels (Thermo Fisher),
431 transferred to PVDF and probed for rabbit anti-human phospho-MLKL (Abcam), monoclonal rat
432 anti-mouse MLKL (WEHI-3H1) (WEHI, made in house), rabbit polyclonal anti-VDAC1
433 (Millipore) and rabbit polyclonal anti-GAPDH (Cell Signaling).

434 **Inflammasome activation**

435 iBMDMs (WT, EspL or EspL_{C47S}) were seeded in 12 well tissue culture treated plates and
436 treated with 50 ng/mL ultra-pure LPS (Invivogen) for 2 h then 1 µg/mL doxycycline (Sigma) added
437 for an additional 2 h. Cells were subsequently stimulated with 1 µM Cp.A (Tetralogic
438 pharmaceuticals) and/or 15 µM QVD-Oph (RnD Systems) for 6 h or 10 µM Nigericin (Sigma) for 1
439 h. Cell supernatants and lysates were analysed by western blot. Primary antibodies used were
440 mouse monoclonal anti-Flag M2-HRP (Sigma), mouse monoclonal caspase-1 (casper-1)
441 (Adipogen), mouse monoclonal anti-RIPK1 (38/RIP) (BD Transduction), rabbit polyclonal RIPK3

442 (Axxora; PSC-2283-C100) and mouse monoclonal anti- β -actin (AC-15) (Sigma). All antibody
443 dilutions were performed in 5% skim milk/0.1% PBS Tween.

444 **IL-8 secretion assay**

445 For analysis of IL-8 secretion, HT-29 cell monolayers were infected for 3 h before being
446 incubated for 8-12 h in media supplemented with 50 μ g/mL gentamicin with or without 20 ng/mL
447 TNF (Calbiochem, EMD4Biosciences, USA). Following this, the HT-29 cell supernatant was
448 collected and either used immediately or stored at -20 $^{\circ}$ C for subsequent analysis of IL-8 secretion.
449 IL-8 secretion was measured using the Human IL-8 ELISA MAX Deluxe Set (Biolegend, CA,
450 USA) according to the manufacturer's instructions.

451 **qRT-PCR**

452 Samples for qRT-PCR experiments were DNase treated using Ambion TURBO DNA-free
453 kit and cDNA synthesis was completed using the iScriptTM cDNA synthesis kit (Bio-Rad). qRT-
454 PCR was performed using SsoAdvancedTM Universal SYBR[®] Green Supermix (Bio-Rad) according
455 to manufacturer's instructions and gene specific primers used are listed in Table S1. Samples were
456 loaded onto MicroAmp[®] Optical 384-well reaction plates (Life technologies) in duplicate and run
457 on the ABI Quant Studio 7 according to manufacturer's instructions. Melting curve analysis was
458 used to ensure there were no primer dimers. Negative controls included both a no-reverse
459 transcriptase control and a no cDNA control. Data were analysed by the threshold cycle method
460 ($\Delta\Delta$ Ct method)³⁸ and normalised to *18S* abundance. All data are represented as fold induction
461 relative to gene expression in uninduced, unstimulated cells or uninfected, unstimulated cells. All
462 experiments were carried out in triplicate.

463 **Beta-lactamase translocation assay**

464 HeLa cells were seeded in black 96 well trays with transparent well bottom (Greiner Bio-
465 One) for 16 to 24 h prior to infection. On the day of infection, EPEC strains with derivatives of
466 pCX340 were cultured as previously described. 2.5 mM Probenecid (Sigma) and 1 mM IPTG

467 (Sigma) were added to bacterial cultures for the last 45 min before infection. HeLa cells were
468 loaded with CCF2/AM substrate following manufacturer's instructions (Invitrogen) and incubated
469 at room temperature in the dark for one hour. 15 minutes before infection, cells were transferred
470 back to 37 °C 5% CO₂. Infection was carried out using 50 µl of bacterial culture with an OD₆₀₀ of
471 0.1 for 60 min at 37 °C in 5% CO₂. Translocation was measured as a ratio of
472 Emission_{450nm}:Emission_{520nm} using a CLARIOstar Omega microplate reader (BMGLabtech) using
473 triplicate wells for each strain.

474 **Dual-luciferase reporter assay**

475 For the NF-κB dual-luciferase assay, HeLa cells were seeded into 24-well trays (Corning)
476 and co-transfected with derivatives of p3xFlag-*Myc*-CMV-24 (0.4 µg), 0.05 µg of pRL-TK
477 (Promega, Madison WI, USA) and 0.2 µg of pNF-κB-Luc (Clontech, Palo Alto CA, USA).
478 Approximately 24 h post-transfection, cells were left untreated or stimulated with 20 ng/mL
479 TNFα (Calbiochem, La Jolla, CA) for 6 h. Firefly and Renilla luciferase levels were measured using
480 the Dual-luciferase reporter assay system (Promega) in a CLARIOstar Omega microplate reader
481 (BMGLabtech, Germany). The expression of firefly luciferase was normalised for Renilla luciferase
482 measurements and Luciferase activity was expressed relative to unstimulated p3xFlag-*Myc*-CMV-
483 24-transfected cells.

484 ***In vitro* cleavage assays**

485 Purified proteins were diluted out of urea-containing buffer and incubated in 100 µl of
486 reaction buffer (25 mM NaH₂PO₄, 150 mM NaCl, 0.5 mM DTT, pH 7.4) at a concentration of 20
487 µM (RHIM proteins) or 0.9 µM (EspL/EspL_{C47S}) for 1 hour at 37 °C. Sample buffer was then added
488 to incubated proteins, before the samples were boiled and subjected to SDS-PAGE on Nu-PAGE 4-
489 12% Bis-Tris polyacrylamide gels. The gels were stained with Coomassie Blue Stain and imaged
490 with a GelMax imager (UVP, Analytik Jena, USA).

491 To compare the cleavage of RHIM-containing protein in monomeric and fibrillar forms,
492 10 µg EspL was added to 200 µL of 20 µM of His-Ub-RIPK3 in 25 mM NaH₂PO₄, 150 mM NaCl,
493 0.5 mM DTT, pH 7.4 immediately following dilution of His-Ub-RIPK3 from 8M urea-containing
494 buffer or after incubation of the diluted His-Ub-RIPK3 for 225 min at 37 °C to allow fibril
495 formation. Samples were subsequently incubated with EspL at 37 °C for 1 h. For both ‘monomer’
496 and ‘fibril’ samples, 100 µL was pelleted at 16,000g for 10 min. The supernatant was collected as
497 the soluble fraction and the pellet was resuspended with 100 µL of 8M urea, pH 4.0. Samples were
498 subjected to SDS-PAGE and stained with Coomassie Blue Stain for visualisation and imaging as
499 above.

500 **Thioflavin-T (ThT) assays**

501
502 Thioflavin-T (ThT) assays were used to monitor fibril formation. 20µM of recombinant
503 RHIM containing His-Ub-RIPK3 was incubated in buffer (25 mM NaH₂PO₄, 150 mM NaCl, 0.5
504 mM DTT, pH 7.4, 40 µM ThT) in a Costar 96-well plate (Corning) at 37 °C for 3.75 hours inside a
505 POLARstar Omega microplate reader (BMGLabtech). Samples were excited at 440 nm and ThT
506 fluorescence emission was measured at 480 nm every 60 seconds. Fibril formation was evident after
507 225 min. To test the cleavage of RHIM fibrils by EspL, 500 µl of 20 µM of His-Ub-RIPK3 was
508 dialysed against 1 L of dialysis buffer (25 mM NaH₂PO₄, 150 mM NaCl, 0.5 mM DTT, pH 7.4) for
509 24 h at room temperature. 100 µl of ‘fibril’ sample was then incubated with 0.9 µM purified EspL,
510 vortexed briefly and incubated at 37 °C for either 1 or 2 h. For both ‘monomer’ and ‘fibril’ samples,
511 100 µl was pelleted at 16,000 g for 10 min. The supernatant was collected as the soluble fraction
512 and the pellet was resuspended with 100 µl of 8M urea, pH 4.0. Samples were subjected to SDS-
513 PAGE and stained with Coomassie Blue Stain for visualisation and imaging as previously
514 mentioned.

515

516

517 **Reverse-phase HPLC**

518 200–1000 μL of purified RHIM proteins at a concentration of 20 μM were incubated with or
519 without 0.9 μM of purified EspL for 1 hour at 37 °C. Proteins were then analysed by RP-HPLC
520 using a C₈ VYDAC column running in MilliQ water containing 0.1% TFA, 10% methanol and
521 eluted with an increasing gradient of acetonitrile. Peaks were collected and lyophilized for further
522 analysis by N-terminal sequencing or LC-MS/MS.

523 **N-terminal sequencing**

524 N-terminal sequencing was performed by the Australian Proteome Analysis Facility (APAF)
525 at Macquarie University, New South Wales, Australia.

526 **Characterisation of His₆-Ub-RIPK3 and His₆-Ub-TRIF cleavage products by intact mass**
527 **spectrometry analysis**

528 Characterisation of RIPK3 and TRIF cleavage products by intact mass spectrometry were
529 performed on samples prepared by *in vitro* cleavage assay and purified by RP-HPLC as described
530 above.

531 *Time-of-flight tandem mass spectrometry*

532 Mass measurements of the intact protein ions and ETD and CID MS/MS were performed on the
533 high resolution, high mass accuracy quadrupole time-of-flight (qTOF) mass spectrometer (maXis II
534 UHR qTOF, Bruker Daltonics, Bremen, Germany) equipped with an electrospray ion (ESI) source
535 for the direct-infusion method. For the direct-infusion experiments a flow rate of 180 $\mu\text{L}/\text{min}$ was
536 provided by a syringe pump (KdScientific, Holliston, MA, USA) using a 25 μL syringe (SGE
537 Analytical Sciences, VIC, AUS). The following settings were applied: capillary voltage of 4.5 kV,
538 end plate offset of 500 V, mass range of m/z 450 to 2500, dry gas of 4.0 L/min, and drying
539 temperature of 220 °C. Nano-ESI infusion was performed using HPLC fractions which were
540 reconstituted in 20 μl of water and diluted 1:10 with 50% acetonitrile: 50% water containing 1%
541 formic acid.

542 *Data analysis*

543 The MS and MS/MS spectra were analyzed using a dedicated top-down data analysis procedure.
544 Briefly, precursor and product ion mass spectra were summed over the infusion time in each MS
545 and MS/MS experiment with Data Analysis software version 4.3 (Bruker Daltonics). Automatic
546 data analysis was performed by deisotoping keeping only the monoisotopic masses followed by
547 charge state deconvolution (SNAP 2 algorithm). The obtained mass list of product ions was
548 matched on the predicted cleaved mRIPK3 sequence to determine the product ion identity and the
549 sequence coverage using the observed mass of the precursor ion.

550 **Necroptosis experiments.** The human epithelial cell line, HT-29, as well as mouse dermal
551 fibroblasts (MDF) and immortalised bone marrow derived macrophages (iBMDMs) either infected
552 with derivatives of EPEC E2348/69 or engineered to express EspL derivatives were used to
553 examine the effect of EspL on necroptosis. Necroptosis was induced by treatment with 1) 20 ng/mL
554 TNF, 500 nM Cp.A and 25 μ M z-VAD-FMK or 50 μ M QVD-OPH or 2) 20 ng/mL of LPS (*E. coli*
555 0111:B4) and 10 μ M z-VAD-FMK or 3) 50 μ g/mL Poly I:C (for iBMDMs) or 10 μ g/mL high
556 molecular weight Poly I:C (for HT-29) and 10 μ M z-VAD-FMK. Cell viability was assessed by
557 reduction of 3-(4,5-Dimethylthiazol-2-yl)-2,5- diphenyltetrazolium bromide (MTT) or by
558 propidium iodide (PI) uptake. MLKL complex formation and membrane translocation were
559 examined by Blue native PAGE of cell membrane and cytosolic fractions and immunoblotting
560 using antibodies to MLKL and phospho-MLKL.

561 **Protein sequence alignment and phylogenetic tree**

562 RHIM domain alignment for human and mouse RIPK1, RIPK3, TRIF and DAI was
563 performed by Clustal Omega and ESPript³⁹. Accession numbers (same order as displayed in Fig.
564 2c) NP_003795, NP_033094, NP_006862, NP_064339, NP_891549, NP_778154, NP_110403,
565 NP_067369, NP_001153889, NP_001132991. For comparison of the cysteine protease motif,
566 sequences were identified through BLAST using EspL from EPEC E2348/69 as a reference. A

567 section of the proteins identified by BLAST were aligned using Clustal Omega and presentation of
568 alignment performed using ESPript3³⁹. Accession numbers (same order as displayed in
569 Supplementary Figure Fig. 2) CAS10778, AIG70345, WP_012905388, WP_031942474,
570 WP_024259347, ENZ84489, WP_023263817, WP_015872003, WP_020957625, CCA83579,
571 WP_009667375, CDG86051, WP_004389152, WP_004714204, WP_019080404, AHK18540,
572 WP_002211641, AIN16488.

573 A set of protein sequences was curated based on the identification of homologues of EspL
574 from EPEC E2348/69. BLAST²⁵ was used to compare these protein sequences to the *nr* database
575 and *nt* database (downloaded on 31st July from <ftp://ftp.ebi.edu.au/pub/databases/ncbi/blast/db/>)
576 with blastp and tblastn respectively to identify additional proteins. The subsequent results were
577 filtered on the E scores of 0.0 and length, and reduced to unique accession (removing duplicates).
578 The nucleotide sequences were translated into amino acid sequences with EMBOSS⁴⁰ and the
579 protein sequences were aligned with Muscle⁴¹. The best fitting protein model was determined using
580 the Perl script ProteinModelSelection.pl available at <http://sco.hits.org/exelixis/web/software/raxml/>
581 for RAxML⁴². One hundred pseudo-replicate RAxML analyses were run three times using the best-
582 fitting substitution model, PROTGAMMA VF. The best scoring Maximum Likelihood tree was
583 selected and midpoint rooted in Dendroscope⁴³. The following accession numbers were used for
584 phylogenetic analyses; CAS10778.1, AIG70345.1, CBG87854.1, ACR69900, CP001064,
585 CP011417, LM996972, LM997319, CP001064, Z54194, WP_028120439, LM996116,
586 WP_028120664, WP_038348374, AJ303141 LM996576, AP010958, LM995478, LM995537,
587 LM996653, LM997233, LM997407, LM995613, LM997087, WP_001121612, WP_001121619,
588 WP_001121621, WP_033810450, WP_044863368, AAJV00000000, AIAN00000000, FM986650,
589 AP010960, LM996367, EHW09036, EHW21689, WP_001121623, WP_001121627,
590 WP_001121746, WP_001121747, WP_001121748, WP_021824236, WP_023981847,
591 WP_032272532, WP_032273780, AIHA00000000, WP_032349748, AIHB00000000,

592 AIHD00000000, AIHE00000000, AAJX00000000, AIBC00000000, LN554915, LM996042,
593 LM996071, LM996922, WP_001121620, WP_032210130, AKNI01000047, AIAL00000000,
594 AIAO00000000, AIGY00000000, AIGZ00000000, AIBX00000000, CP006262, CP007133,
595 LM996313, LM996458, CP007136, LM995993, LM996803, LM997001, WP_001121622,
596 AIAI00000000, AIAX00000000, AF453441, AIBD00000000, CP008805, CP001164, CP001368,
597 CP001925, CP010304, EHV10408, WP_001121626, WP_024256897, WP_032208682,
598 AIAQ00000000, LM995690, LM995751, LM995947, AJ277443, FM201463, LM995831,
599 LM996694, LM997125, EHW62569, WP_001121617, WP_032345473, WP_045889142,
600 AICF00000000, AIAC00000000, AIGK00000000, AIGN00000000, AIGO00000000,
601 AIAG00000000, AIGL00000000, AIGM00000000, AIBT00000000, AIBR00000000,
602 AIBV00000000, AIGX00000000, WP_001121628, CP001846, CP003109, WP_001121608,
603 WP_001121609, WP_001121624, AIAH00000000, AIAD00000000, ADUL01000000,
604 AIFD00000000, AIAE00000000, AIFS00000000, AIFT00000000, AIFU00000000,
605 AIFQ00000000, FM986652, LM996749, CDG86051, WP_038497945, WP_009667375,
606 CCA83579, FP885907, AEG72234, CBJ36034, CEJ16658, EUJ11993, WP_003265371,
607 WP_003274329, WP_013209029, WP_039553678, WP_042549988, WP_042592182,
608 WP_043947056, ENZ84489, CP000037, CP001062, WP_012421777, CP000035, CP006737,
609 ADA76828, EFP73031, EFW48342, WP_000608472, WP_005015229, WP_011379052,
610 AY879342, NG_035859, NG_035867, AF348706, AF386526, AL391753, AY879342, CP001384,
611 CP007038, Z54211, CAA90938, EIQ30821, WP_005058548, WP_005061014, WP_005065444,
612 WP_005115993, WP_005117432, WP_010921597, WP_010921642, WP_015060143,
613 WP_024259347, WP_025746267, WP_025748914, WP_025759433, WP_025766126,
614 WP_031942474, WP_039060413, WP_040234710, WP_047204882, WP_047204897, CP000039,
615 CP011423, HE616529, WP_005041841, WP_005138925, WP_024261348, CFB70006,
616 CFQ67145, CNC44257, CRE36360, WP_019080404, CFR06093, WP_004389152, CP000305,

617 CP001585, CP001589, CP001608, CP002956, CP009492, CP009704, CP009723, CP009785,
618 CP009836, CP009844, CP009973, CP009996, CP010023, CP010293, AE009952, AE017042,
619 AL590842, CP000308, CP001593, CP009840, CP009906, CP009991, KGA51839,
620 WP_002211641, WP_045123609, BX936398, CP001048, CP009757, CP009780, CP009786,
621 CP010067, CP000950, CP008943, CP009712, CP009759, CP009792, CFV36814, CNG55237,
622 CNJ16181, WP_011193035, WP_012104544, WP_012303595, ESJ22116.1, WP_032466541,
623 WP_038400874, WP_004714204, CP007230, CNC46702, WP_025381344, WP_006576111.1

624 **Mouse infection studies**

625 All animal experimentation was approved by the Melbourne University Animal Ethics
626 Committee. All mice used were of a C57BL/6 background and were age matched as best as possible
627 between 5-8 weeks pre-infection. No calculation was used to assess the number of animals required.
628 Male and female mice were allocated to experimental groups to ensure even distribution of age, sex
629 and weight and investigators were not blinded to the allocation. *Citrobacter rodentium* was cultured
630 in LB broth overnight before centrifugation and re-suspension in PBS to a concentration of $\sim 5 \times 10^9$
631 cells/mL. C57BL/6 (5- to 8 weeks old) were inoculated by oral gavage with 200 μ l of
632 approximately 1×10^9 c.f.u of *C. rodentium*. The viable count of the inoculum was determined
633 retrospectively by plating dilutions of the inoculum on plates with appropriate antibiotics. Mice
634 were weighed every 2 days and faeces collected every 2 or 4 days for enumeration of c.f.u. The
635 viable count per g of faeces was determined by plating serial dilutions of faeces onto media
636 containing selective antibiotics.

637 **Statistical analysis.** All statistical analyses were performed using GraphPad Prism version 6.0.
638 Statistical tests used were unpaired two-tailed Student's *t*-test for pairwise comparisons between
639 groups or One-way ANOVA with Holm-Sidak's Test for multiple comparisons where indicated.
640 Variance was similar in all comparisons. Differences in faecal counts of CR from mice and

641 diarrhoea and pathology scores were assessed using a Mann Whitney U test, where normal
642 distribution was not assumed. $P < 0.05$ was considered to be significant.

643 **Data availability.** The data that support the findings of this study are available from the
644 corresponding author upon request

645

647 **References**

- 648 1 Sun, X., Yin, J., Starovasnik, M. A., Fairbrother, W. J. & Dixit, V. M. Identification of a
649 novel homotypic interaction motif required for the phosphorylation of receptor-interacting
650 protein (RIP) by RIP3. *J Biol Chem* **277**, 9505-9511 (2002).
- 651 2 Kaiser, W. J. & Offermann, M. K. Apoptosis induced by the toll-like receptor adaptor TRIF
652 is dependent on its receptor interacting protein homotypic interaction motif. *J Immunol* **174**,
653 4942-4952 (2005).
- 654 3 Rebsamen, M. *et al.* DAI/ZBP1 recruits RIP1 and RIP3 through RIP homotypic interaction
655 motifs to activate NF-kappaB. *EMBO Rep* **10**, 916-922 (2009).
- 656 4 Li, J. *et al.* The RIP1/RIP3 necrosome forms a functional amyloid signaling complex
657 required for programmed necrosis. *Cell* **150**, 339-350 (2012).
- 658 5 Pasparakis, M. & Vandenabeele, P. Necroptosis and its role in inflammation. *Nature* **517**,
659 311-320 (2015).
- 660 6 Micheau, O. & Tschopp, J. Induction of TNF receptor I-mediated apoptosis via two
661 sequential signaling complexes. *Cell* **114**, 181-190 (2003).
- 662 7 Holler, N. *et al.* Fas triggers an alternative, caspase-8-independent cell death pathway using
663 the kinase RIP as effector molecule. *Nat Immunol* **1**, 489-495 (2000).
- 664 8 Cho, Y. S. *et al.* Phosphorylation-driven assembly of the RIP1-RIP3 complex regulates
665 programmed necrosis and virus-induced inflammation. *Cell* **137**, 1112-1123 (2009).
- 666 9 He, S. *et al.* Receptor interacting protein kinase-3 determines cellular necrotic response to
667 TNF-alpha. *Cell* **137**, 1100-1111 (2009).
- 668 10 Murphy, J. M. *et al.* The pseudokinase MLKL mediates necroptosis via a molecular switch
669 mechanism. *Immunity* **39**, 443-453 (2013).
- 670 11 Sun, L. *et al.* Mixed lineage kinase domain-like protein mediates necrosis signaling
671 downstream of RIP3 kinase. *Cell* **148**, 213-227 (2012).
- 672 12 Cai, Z. *et al.* Plasma membrane translocation of trimerized MLKL protein is required for
673 TNF-induced necroptosis. *Nat Cell Biol* **16**, 55-65 (2014).
- 674 13 Hildebrand, J. M. *et al.* Activation of the pseudokinase MLKL unleashes the four-helix
675 bundle domain to induce membrane localization and necroptotic cell death. *Proc Natl Acad*
676 *Sci U S A* **111**, 15072-15077 (2014).
- 677 14 Kaiser, W. J. *et al.* Toll-like receptor 3-mediated necrosis via TRIF, RIP3, and MLKL. *J*
678 *Biol Chem* **288**, 31268-31279 (2013).
- 679 15 Upton, J. W., Kaiser, W. J. & Mocarski, E. S. DAI/ZBP1/DLM-1 complexes with RIP3 to
680 mediate virus-induced programmed necrosis that is targeted by murine cytomegalovirus
681 vIRA. *Cell Host Microbe* **11**, 290-297 (2012).
- 682 16 Lawlor, K. E. *et al.* RIPK3 promotes cell death and NLRP3 inflammasome activation in the
683 absence of MLKL. *Nat Commun* **6**, 6282 (2015).
- 684 17 Giogha, C., Lung, T. W., Pearson, J. S. & Hartland, E. L. Inhibition of death receptor
685 signaling by bacterial gut pathogens. *Cytokine Growth Factor Rev* **25**, 235-243 (2014).
- 686 18 Pearson, J. S. *et al.* A type III effector antagonizes death receptor signalling during bacterial
687 gut infection. *Nature* **501**, 247-251 (2013).
- 688 19 Li, S. *et al.* Pathogen blocks host death receptor signalling by arginine GlcNAcylation of
689 death domains. *Nature* **501**, 242-246 (2013).
- 690 20 Zhang, L. *et al.* Cysteine methylation disrupts ubiquitin-chain sensing in NF-kappaB
691 activation. *Nature* **481**, 204-208 (2012).

- 692 21 Charpentier, X. & Oswald, E. Identification of the secretion and translocation domain of the
693 enteropathogenic and enterohemorrhagic *Escherichia coli* effector Cif, using TEM-1 beta-
694 lactamase as a new fluorescence-based reporter. *J Bacteriol* **186**, 5486-5495 (2004).
- 695 22 Wertz, I. E. *et al.* De-ubiquitination and ubiquitin ligase domains of A20 downregulate NF-
696 kappaB signalling. *Nature* **430**, 694-699 (2004).
- 697 23 Newton, K. *et al.* Ubiquitin chain editing revealed by polyubiquitin linkage-specific
698 antibodies. *Cell* **134**, 668-678 (2008).
- 699 24 Lin, Y., Devin, A., Rodriguez, Y. & Liu, Z. G. Cleavage of the death domain kinase RIP by
700 caspase-8 prompts TNF-induced apoptosis. *Genes Dev* **13**, 2514-2526 (1999).
- 701 25 Altschul, S. F., Gish, W., Miller, W., Myers, E. W. & Lipman, D. J. Basic local alignment
702 search tool. *J Mol Biol* **215**, 403-410 (1990).
- 703 26 Kelley, L. A. & Sternberg, M. J. Protein structure prediction on the Web: a case study using
704 the Phyre server. *Nat Protoc* **4**, 363-371 (2009).
- 705 27 Shao, F., Merritt, P. M., Bao, Z., Innes, R. W. & Dixon, J. E. A *Yersinia* effector and a
706 *Pseudomonas* avirulence protein define a family of cysteine proteases functioning in
707 bacterial pathogenesis. *Cell* **109**, 575-588 (2002).
- 708 28 Humphries, F., Yang, S., Wang, B. & Moynagh, P. N. RIP kinases: key decision makers in
709 cell death and innate immunity. *Cell Death Differ* **22**, 225-236 (2015).
- 710 29 Vince, J. E. *et al.* IAP antagonists target cIAP1 to induce TNFalpha-dependent apoptosis.
711 *Cell* **131**, 682-693 (2007).
- 712 30 Wickham, M. E. *et al.* Bacterial genetic determinants of non-O157 STEC outbreaks and
713 hemolytic-uremic syndrome after infection. *J Infect Dis* **194**, 819-827 (2006).
- 714 31 Conzen, S. D. & Cole, C. N. The three transforming regions of SV40 T antigen are required
715 for immortalization of primary mouse embryo fibroblasts. *Oncogene* **11**, 2295-2302 (1995).
- 716 32 Hornung, V. *et al.* Silica crystals and aluminum salts activate the NALP3 inflammasome
717 through phagosomal destabilization. *Nat Immunol* **9**, 847-856 (2008).
- 718 33 Tanzer, M. C. *et al.* Evolutionary divergence of the necroptosis effector MLKL. *Cell Death*
719 *Differ* **23**, 1185-1197 (2016).
- 720 34 Catanzariti, A. M., Soboleva, T. A., Jans, D. A., Board, P. G. & Baker, R. T. An efficient
721 system for high-level expression and easy purification of authentic recombinant proteins.
722 *Protein Sci* **13**, 1331-1339 (2004).
- 723 35 Galan, J. E., Ginocchio, C. & Costeas, P. Molecular and functional characterization of the
724 Salmonella invasion gene invA: homology of InvA to members of a new protein family. *J*
725 *Bacteriol* **174**, 4338-4349 (1992).
- 726 36 Datsenko, K. A. & Wanner, B. L. One-step inactivation of chromosomal genes in
727 *Escherichia coli* K-12 using PCR products. *Proc Natl Acad Sci U S A* **97**, 6640-6645.
728 (2000).
- 729 37 McKenzie, G. J. & Craig, N. L. Fast, easy and efficient: site-specific insertion of transgenes
730 into enterobacterial chromosomes using Tn7 without need for selection of the insertion
731 event. *BMC Microbiol* **6**, 39 (2006).
- 732 38 Huang, K. F., Chiou, S. H., Ko, T. P., Yuann, J. M. & Wang, A. H. The 1.35 A structure of
733 cadmium-substituted TM-3, a snake-venom metalloproteinase from Taiwan habu:
734 elucidation of a TNFalpha-converting enzyme-like active-site structure with a distorted
735 octahedral geometry of cadmium. *Acta Crystallogr D Biol Crystallogr* **58**, 1118-1128
736 (2002).
- 737 39 Gouet, P., Courcelle, E., Stuart, D. I. & Metz, F. ESPript: analysis of multiple sequence
738 alignments in PostScript. *Bioinformatics* **15**, 305-308 (1999).
- 739 40 Coppolino, M. G. *et al.* Requirement for N-ethylmaleimide-sensitive factor activity at
740 different stages of bacterial invasion and phagocytosis. *J Biol Chem* **276**, 4772-4780 (2001)

741 41 Edgar, R. C. MUSCLE: a multiple sequence alignment method with reduced time and space
742 complexity. *BMC Bioinformatics* **5**, 113 (2004).

743 42 Stamatakis, A. RAxML version 8: a tool for phylogenetic analysis and post-analysis of large
744 phylogenies. *Bioinformatics* **30**, 1312-1313 (2014).

745 43 Huson, D. H. & Scornavacca, C. Dendroscope 3: an interactive tool for rooted phylogenetic
746 trees and networks. *Syst Biol* **61**, 1061-1067 (2012).

747 44 Levine, M. M. *et al.* Escherichia coli strains that cause diarrhoea but do not produce heat-
748 labile or heat-stable enterotoxins and are non-invasive. *Lancet* **1**, 1119-1122 (1978).

749 45 Newton, H. J. *et al.* The type III effectors NleE and NleB from enteropathogenic *E. coli* and
750 OspZ from *Shigella* block nuclear translocation of NF-kappaB p65. *PLoS Pathog* **6**,
751 e1000898 (2010).

752 46 Garmendia, J. *et al.* TccP is an enterohaemorrhagic *Escherichia coli* O157:H7 type III
753 effector protein that couples Tir to the actin-cytoskeleton. *Cell Microbiol* **6**, 1167-1183
754 (2004).

755 47 Mundy, R. *et al.* Identification of a novel type IV pilus gene cluster required for
756 gastrointestinal colonization of *Citrobacter rodentium*. *Mol Microbiol* **48**, 795-809 (2003).

757 48 Kelly, M. *et al.* Essential role of the type III secretion system effector NleB in colonization
758 of mice by *Citrobacter rodentium*. *Infect Immun* **74**, 2328-2337 (2006).

759 49 Yamamoto, M. *et al.* A cluster of interferon-gamma-inducible p65 GTPases plays a critical
760 role in host defense against *Toxoplasma gondii*. *Immunity* **37**, 302-313 (2012)

761

762

763

764 **Legend to the figures**

765 **Figure 1. EspL is a T3SS cysteine protease that degrades RIPK1 and RIPK3. a,** Schematic

766 representation of EPEC E2348/69 genomic integrative element 6 (IE6) harbouring *espL*, *nleB1*, and

767 *nleE* and immunoblot showing RIPK1 degradation in HT-29 cells infected with derivatives of

768 EPEC E2348/69 as shown. Representative immunoblot from at least 3 independent experiments.

769 Actin; loading control. **b,** Immunoblot showing RIPK1 degradation in HeLa cells uninfected or

770 infected with EPEC E2348/69; untreated, or treated with either MG132 or z-VAD-FMK (z-VAD).

771 Representative immunoblot from at least three independent experiments. Actin; loading control. **c,**

772 Schematic representation of cysteine protease motif and secondary structure predicted by Phyre in

773 YopT from *Y. pestis* KIM and EspL from EPEC E2348/69. **d,** Immunoblot showing levels of

774 RIPK1, RIPK2 and RIPK3 in HT-29 cells infected with derivatives of EPEC E2348/69.

775 Representative immunoblot from at least three independent experiments. Actin; loading control.

776

777 **Figure 2. Distribution of EspL in Gram negative pathogens and substrate specificity. a,**

778 Phylogeny of EspL homologues from a range of Gram negative pathogens which was midpoint

779 rooted. Different genera are highlighted by background colour and the tips are coloured by species

780 or pathotype. **b,** Coomassie Brilliant Blue stain of SDS PAGE gel showing *in vitro* cleavage of

781 purified RHIM-containing regions of RIPK1, RIPK3, TRIF and ZBP1 (expressed as recombinant

782 His₆-ubiquitin-tagged proteins) by purified recombinant EspL. Representative gel from at least two

783 independent experiments. Purified recombinant EspL_{C47S} was used as a negative control. White

784 arrows indicate cleavage products. Black arrows indicate EspL and the band corresponding to free

785 His₆-ubiquitin (His-Ub) Note, observed cleavage product derived from ZBP1/DAI was consistent

786 with EspL cleavage in first RHIM of ZBP1/DAI. **c,** EspL cleavage site indicated by an arrow in the

787 RHIM containing regions of RIPK1, RIPK3, TRIF and ZBP1/DAI. Alignment was performed using

788 Clustal Omega and ESPript3. Cleavage sites in RIPK3 and TRIF were determined experimentally
789 by mass spectrometry and N-terminal sequencing.

790

791 **Figure 3. EspL inhibits TNF-induced necroptosis. a,** Cell death visualised by propidium iodide
792 (PI) staining in HT-29 cells infected with derivatives of EPEC and treated with TNF, compound A
793 (Cp.A) and z-VAD-FMK (z-VAD). Hoechst; stain for nucleic acid. Scale bar, 20 μ m.
794 Representative images shown from at least three independent experiments. **b,** Quantification of PI
795 staining from microscopic analysis in HT-29 cells infected with derivatives of EPEC E2348/69 and
796 treated with TNF, Cp.A and z-VAD. Results are mean \pm s.e.m. percentage of cells positive for PI
797 staining from three independent experiments counting \sim 200 cells in triplicate. * P <0.0001 compared
798 to EPEC E2348/69 infected cells, one-way ANOVA with Holm-Sidak multiple comparison. **c,** Blue
799 native PAGE analysis of MLKL membrane translocation in HT-29 cells infected with derivatives of
800 EPEC E2348/69 treated with TNF, Cp.A and z-VAD. Representative immunoblot from at least
801 three independent experiments. GAPDH; cytosolic fraction loading control, VDAC; membrane
802 fraction loading control.

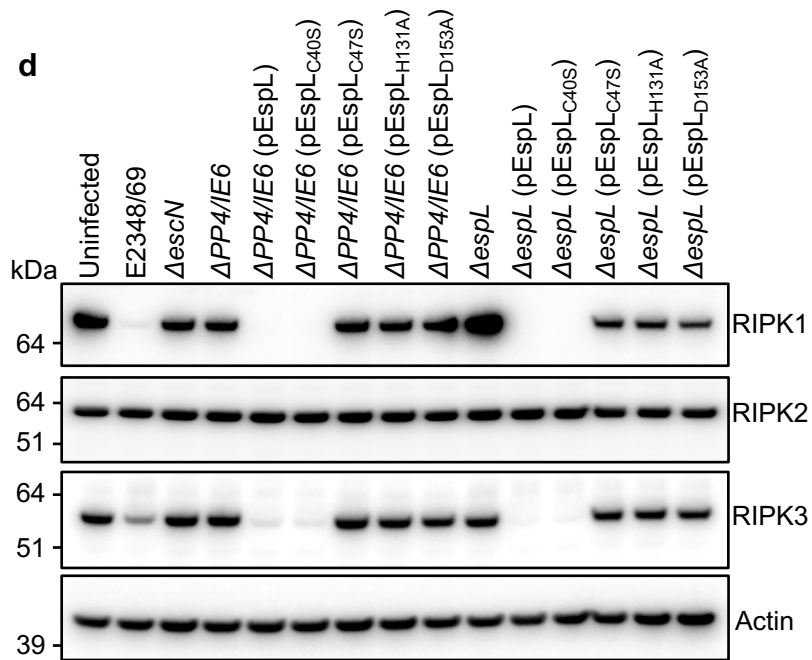
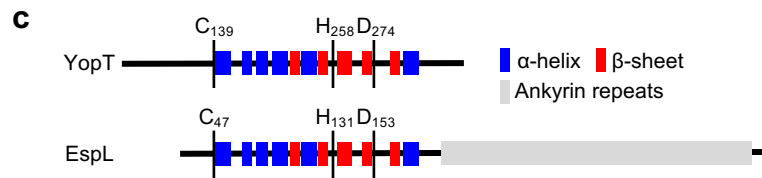
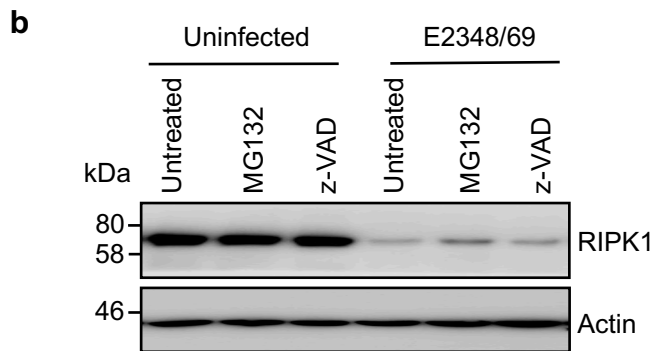
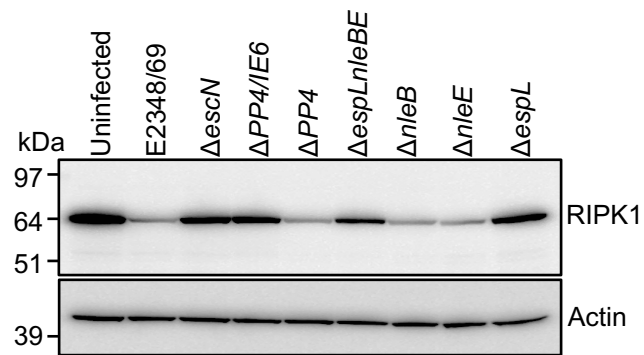
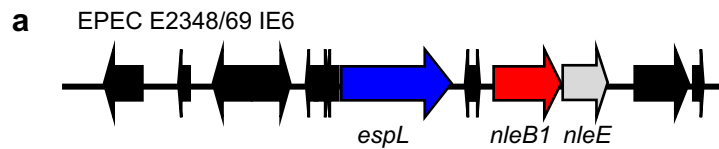
803

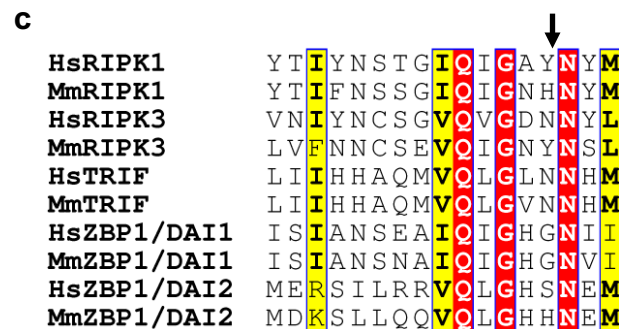
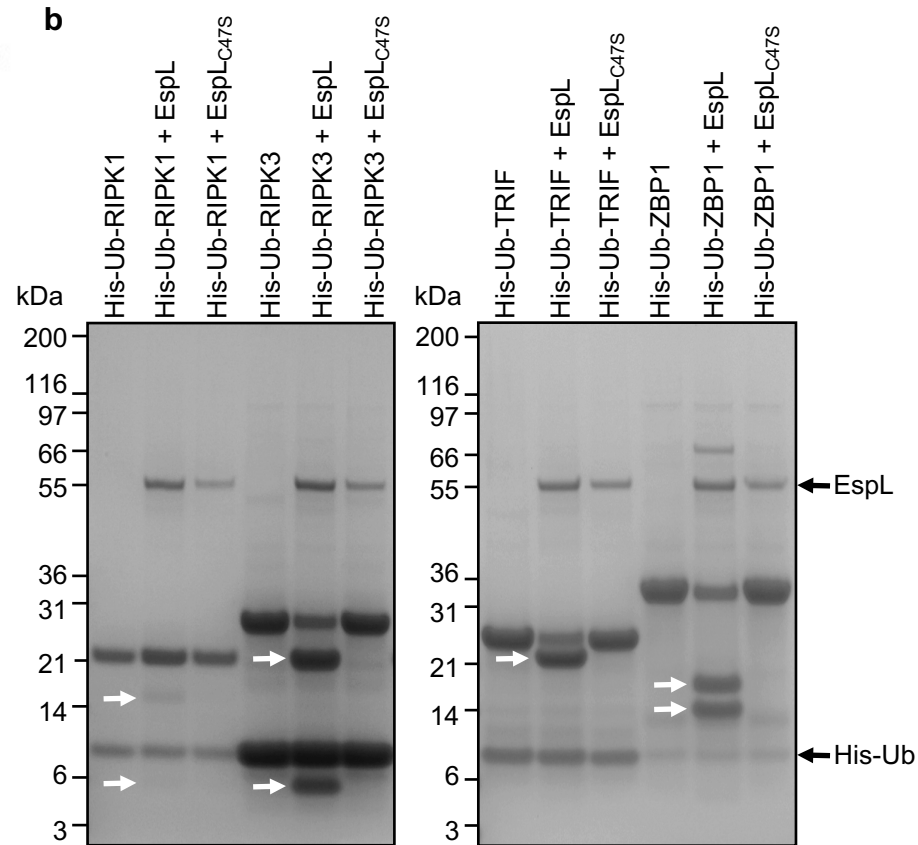
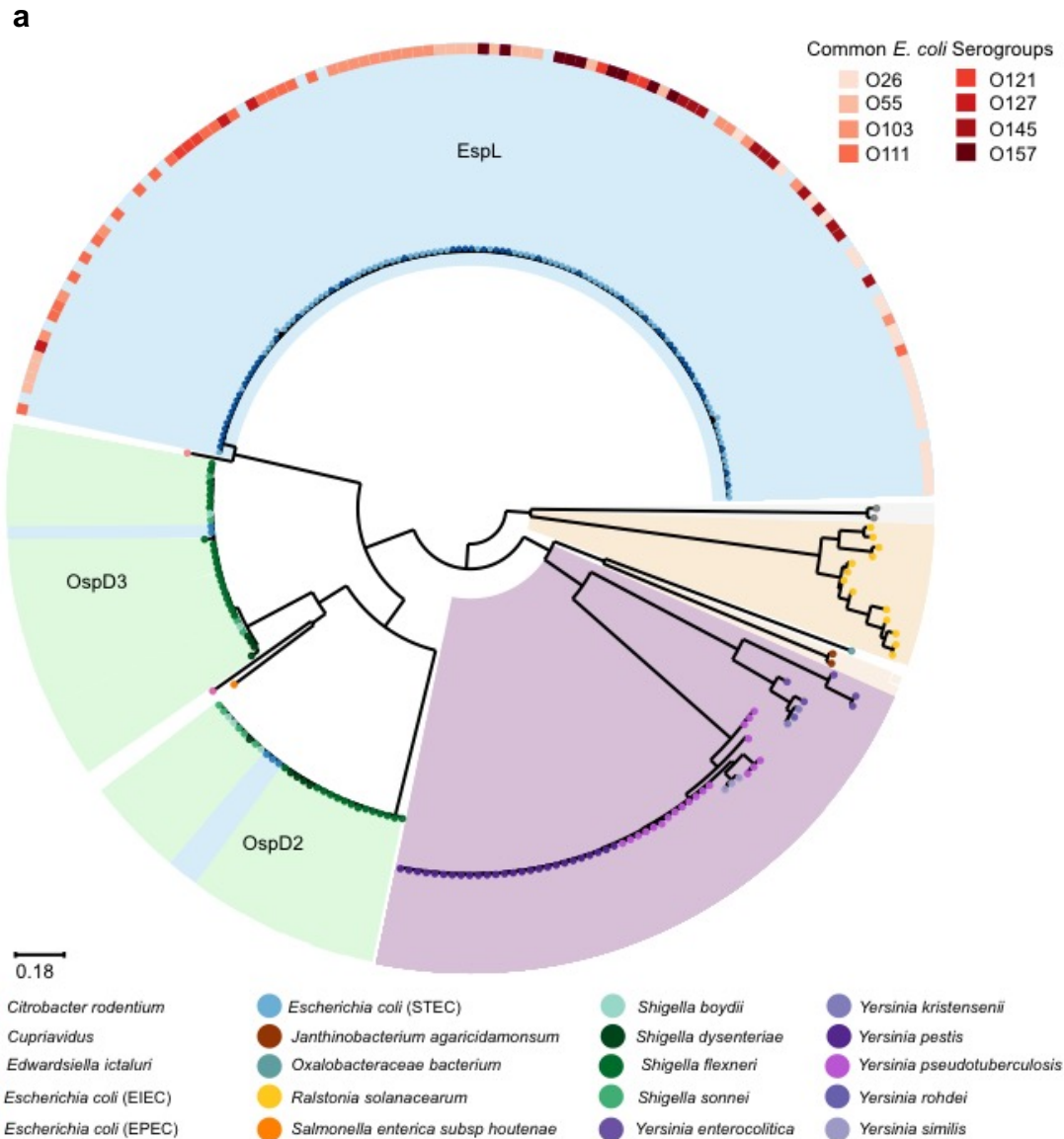
804 **Figure 4. EspL activity inhibits TLR3/4-mediated signalling and contributes to *in vivo***
805 **persistence. a,** *Ifn β* expression in doxycycline-inducible iBMDMs stably expressing either Flag-
806 EspL or Flag-EspL_{C47S} and treated with either LPS or Poly I:C for 3 h as indicated. Results are mean
807 \pm s.e.m of at least three independent experiments performed in triplicate. *Ifn β* expression relative to
808 uninduced, unstimulated cells. * P <0.0005 compared to Flag-EspL induced with doxycycline and
809 treated with LPS or poly I:C, unpaired, two-tailed *t*-test. **b,** MTT reduction in doxycycline-inducible
810 iBMDMs stably expressing either Flag-EspL or Flag-EspL_{C47S} and treated with either LPS/z-VAD
811 or Poly I:C/z-VAD for 20 h. Results are mean \pm s.e.m. of absorbance at 540 nm from three
812 independent experiments performed in triplicate. * P < 0.05 compared to Flag-EspL_{C47S} induced with

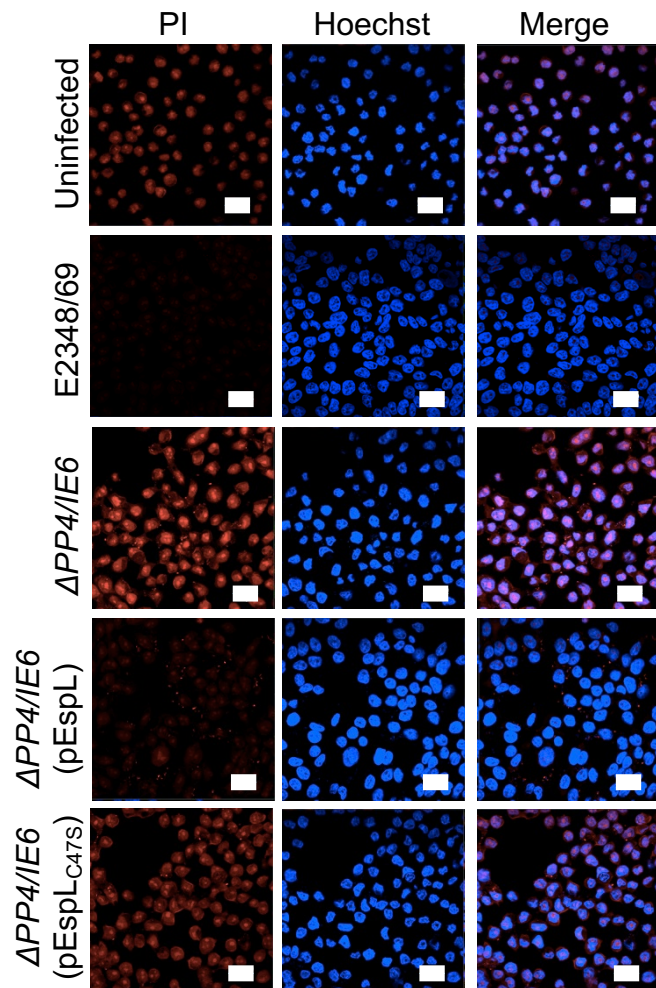
813 doxycycline and treated with LPS or poly I:C, unpaired, two-tailed *t*-test. **c**, Immunoblot showing
814 degradation of endogenous RIPK1 by EspL from *C. rodentium* (Flag-CREspL) but not EspL_{C42S}
815 (Flag-CREspL_{C42S}) expressed ectopically in HEK293T cells. Representative immunoblot from at
816 least three independent experiments. **d**, Bacterial load in the faeces of mice 16 days after infection
817 with derivatives of *C. rodentium*, including wild type *C. rodentium* ICC169 (CR), an *espL* deletion
818 mutant ($\Delta espL$) and $\Delta espL$ complemented with *espL* (EspL) or *espL*_{C42S} (EspL_{C42S}) by Tn7
819 transposition. Each data point represents log₁₀ c.f.u. per g faeces per individual animal (c.f.u.,
820 colony forming units). Mean \pm s.e.m. are indicated. Data was combined from three independent
821 experiments. *P* values from Mann–Whitney U-test.

822

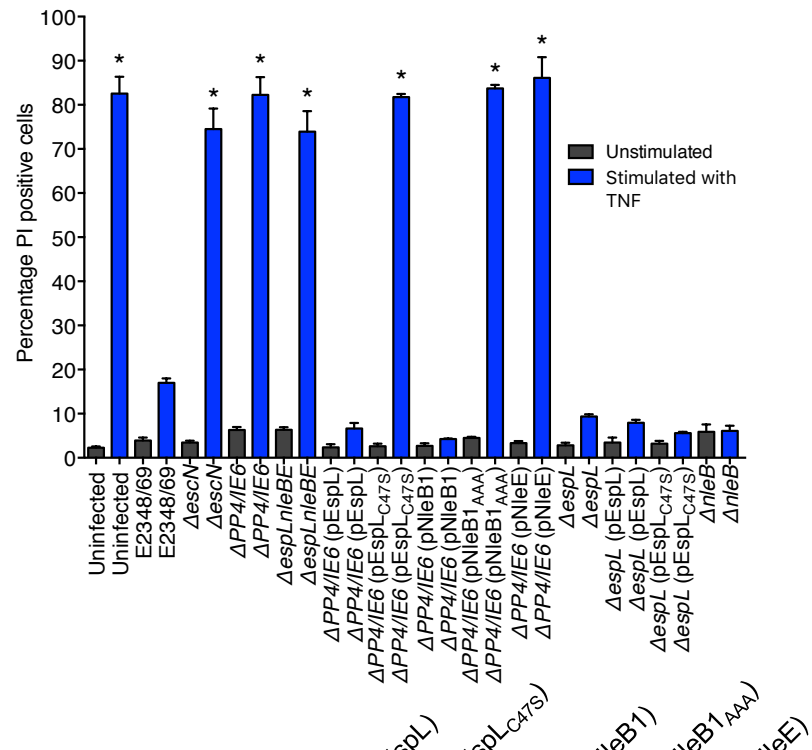
823





a

+ TNF/Cp.A/z-VAD

b**c**